Journal of Optics

PAPER

# Broadband generation of rational-order optical vortices using a bilateral meta-grating

To cite this article: Kun Huang *et al* 2021 *J. Opt.* **23** 024002

View the article online for updates and enhancements.

IOP ebooks™

Bringing together innovative digital publishing with leading authors from the global scientific community.

Start exploring the collection–download the first chapter of every title for free.

This content was downloaded from IP address 114.214.201.181 on 01/07/2021 at 08:38

IOP Publishing Journal of Optics
J. Opt. **23** (2021) 024002 (8pp) https://doi.org/10.1088/2040-8986/abe01e

# Broadband generation of rational-order optical vortices using a bilateral meta-grating

**Kun Huang**[1,3], **Hong Liu**[2,3] **and Jinghua Teng**[2,*]

[1] Department of Optics and Optical Engineering, University of Science and Technology of China, Hefei, Anhui 230026, People's Republic of China
[2] Institute of Materials and Research of Engineering, Agency for Science, Technology and Research, 2 Fusionopolis Way, #08-03, Innovis, Singapore 138634, Singapore

E-mail: jh-teng@imre.a-star.edu.sg

Received 30 November 2020, revised 3 January 2021
Accepted for publication 26 January 2021
Published 12 March 2021

**Abstract**

Optical vortices usually carry integer orbital angular momentum (OAM) of light. Recently, optical vortices with rational-order OAMs have also been created continuously for entangling the super-position OAM states of monochromatic light in a single device. Here, we report the broadband generation of such rational-order optical vortex beams by using a bilateral meta-grating. The meta-grating contains two oblique gratings that encode two sign-opposite linear phase profiles in two symmetric sides, thus leading to phase dislocation along the symmetric axis. We reveal that the encoded phase profiles are valid in a range of wavelengths due to the broadband response of the meta-grating. The measured phase, intensity and tilting angles match perfectly with theoretical prediction, suggesting the bilateral meta-grating as a powerful device to create broadband and continuous OAM of light for various applications such as optical micro-manipulation, optical communication, quantum physics, and super-resolution imaging.

Keywords: optical vortices, gratings, orbital angular momentum, micro-structures, rational-order

(Some figures may appear in colour only in the online journal)

## 1. Introduction

Photons carry spin and orbital angular momenta that are related with the circular polarization and helical wavefront of light, respectively [1]. The spin angular momentum of light takes the value of $\pm\hbar$ ($\hbar$ is the reduced Planck constant), where the sign $\pm$ depends on the handedness of circular polarization [2]. Although both spins are orthogonal, the binary-value property limits their applications in spin Hall effects of light [3, 4], geometric metasurfaces [5], and circular dichroism spectroscopy [6]. In contrast, the orbital angular momentum (OAM) of light has the theoretically unlimited value of $m\hbar$ per photon ($m$ is usually an integer) [7], which offers the multi-dimensional orthogonal bases for optical communication [8, 9] and quantum entanglement [10, 11]. The macroscopic counterpart of the OAM of light refers to optical doughnut-shape vortex beams with the helical phase of $e^{im\varphi}$, where $\varphi$ is the azimuthal coordinate. The ring radius of optical vortex beam increases linearly as the increasing $m$ [12], leading to the large mode volume in various applications. Therefore, the fractional-order optical vortices have gained increasing attention for realizing highly effective dimensionality [13]. In most approaches, the fractional optical vortices are created by making $m$ as a fraction $m_f$, which yields the phase dislocation and the dark intensity at the line of $\varphi = 0$ [14]. Once the fraction $m_f$ changes, the entire phase must be re-distributed along the azimuthal direction. It leads to the fact that one device with a

[3] K. H. and H. L. contributed equally to this work.
[*] Author to whom any correspondence should be addressed.

 © 2021 IOP Publishing Ltd Printed in the UK

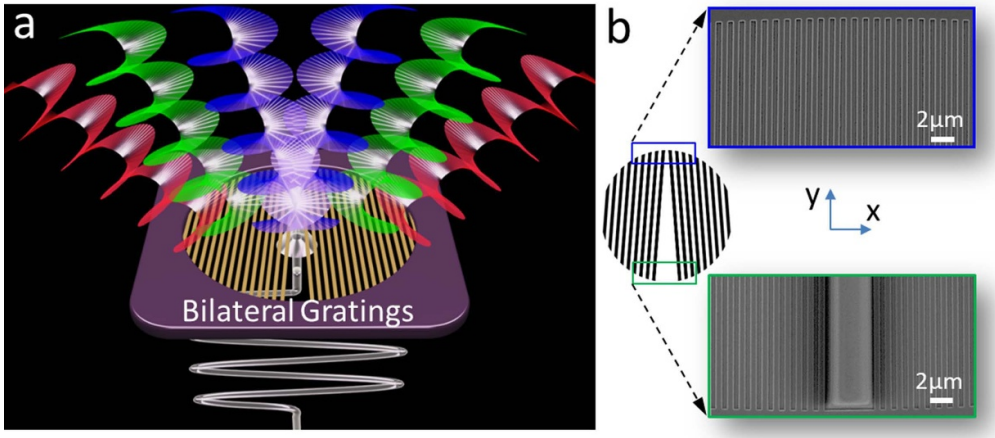


**Figure 1.** (a) Sketch for the broadband creation of optical vortices by using a bilateral gratings. (b) The SEM images of the fabricated samples.

given phase can only create one vortex beam, so that the continuous generation of the fractional-order vortex is challenging in this configuration.

Recently, the mechanism to realize continuously varying rational number OAMs has been proposed by controlling the number of phase singularities that are spatially distributed in a straight line, or a spiniform phase [15]. Thus, one can tune the size of the incident beam smoothly to embrace the number-varied phase singularities so as to realize the continuous generation of rational-order optical vortices in a single device. Since the phase profiles encoded in the designed micro-structures are sensitive to the operating wavelength, a broadband response of such device is important to extend its usage to various laser systems and applications in optics and quantum physics.

Here, we report the creation of broadband rational-order optical vortices by using a single bilateral meta-grating. Based on the rigorous mathematical derivations, we predict theoretically that the encoded phase and optical efficiency are independent on the wavelength, which has been verified by the measured broadband vortices, interference patterns, and nearly constant diffraction efficiencies. Similar to traditional gratings, the broadband optical vortices have the wavelength-dependent diffraction angles, as confirmed in both simulation and experiment. These results could be extended to other electromagnetic waves, acoustic waves and matter waves.

## 2. Theoretical analysis

We begin with the mathematical description of the proposed bilateral meta-grating, as sketched in figure 1(a). The meta-grating is composed of two 1 $\mu$m-period gratings with a tilting angle $\gamma$ and made in an opaque film on a transparent substrate. Although the half-pitch of 500 nm in the meta-grating might induce the subwavelength effects such as polarization modulation and wavelength-dependent transmission, these effects are weak due to the large period of the meta-grating [16] and ignored in our theoretical model. Therefore, the binary-amplitude modulation is employed in this meta-grating, where the amplitude is 1 at the etched parts and 0 at the opaque film. The transmission of the meta-grating can be expressed as [15]

$$\begin{aligned} T(x,y) &= \frac{1}{2} + \sum_{n=1}^{\infty} \mathrm{sinc}\left(n-\frac{1}{2}\right) \\ &\quad \times \cos\{(2n-1)\cdot[\kappa_x x - \mathrm{sgn}(x)\,\beta y]\} \\ &= \frac{1}{2} + \frac{1}{2}\sum_{n=1}^{\infty} \mathrm{sinc}\left(n-\frac{1}{2}\right) \\ &\quad \times \exp\{i\cdot(2n-1)\cdot[\kappa_x x - \mathrm{sgn}(x)\,\beta y]\} \\ &\quad + \frac{1}{2}\sum_{n=1}^{\infty} \mathrm{sinc}\left(n-\frac{1}{2}\right) \\ &\quad \times \exp\{-i\cdot(2n-1)\cdot[\kappa_x x - \mathrm{sgn}(x)\,\beta y]\} \\ &= A_0 + \sum_{n=1}^{\infty} A_{2n-1}\exp\{i\cdot(2n-1)\cdot[\kappa_x x - \mathrm{sgn}(x)\,\beta y]\} \\ &\quad + \sum_{n=1}^{\infty} A_{-(2n-1)}\exp\{-i\cdot(2n-1)\cdot[\kappa_x x - \mathrm{sgn}(x)\,\beta y]\} \end{aligned} \tag{1}$$

where $A_0 = 0.5$, $A_{\pm\ (2n-1)} = 0.5\cdot\mathrm{sinc}(n - 1/2)$ and $\mathrm{sinc}(x) = \sin(x\pi)/(x\pi)$, the odd-order diffraction of transmitted light is labelled by $\pm(2n-1)$, $\mathrm{sgn}(x)$ denotes the sign of the viable $x$ and is responsible for the bilateral symmetry of this meta-grating. The parameters $\kappa_x$ and $\beta$ are related with the period $\Lambda$ and the tilting angle $\gamma$ of the meta-grating: $\Lambda = 2\pi/({\kappa_x}^2 + \beta^2)^{1/2}$ and $\gamma = \arctan(\beta/\kappa_x)$.

The item $\mathrm{sgn}(x)\beta y$ describes the expected phase with the dislocation located along the $y$ axis, because the phase difference between the positive and negative $x$ axis is $\pi$ that is caused by the $\mathrm{sgn}(x)$. To obtain the high-accuracy phase modulation along $y$ direction, the parameter $\beta$ should be sufficiently small, thus resulting in the small tilting angle $\gamma$.

The small $\beta$ has two-fold significances. Firstly, it makes the $y$-direction period ($2\pi/[(2n-1)\beta]$) of meta-grating quite large so that the $y$-direction diffraction of light can be ignored in the theoretical analysis. Thus, the transmitted light obtains a pure phase modulation of $\mathrm{sgn}(x)\beta y$, which has no dependence on the wavelength due to the fixed $\beta$ and therefore enables the broadband response. Secondly, the item $(2n-1)\cdot\kappa_x x$ determines the main structure of the meta-grating. For example, the period of the meta-grating is determined by $\Lambda \approx 2\pi/\kappa_x$ because $\kappa_x$ is much larger than $\beta$. Its transmitted light will take an additional linear phase of $(2n-1)\cdot\kappa_x x$, yielding a $x$-direction linear momentum that leads to the inclination of the transmitted beam. From the viewpoint of light propagation in free space, the phase of a tilting beam can also be described by using the phase item of $\exp[i2\pi/\lambda \sin\theta \cdot x]$, where $\lambda$ is the wavelength of light, $\theta$ is the angle between $z$ axis and the tilted propagation direction of light. The momentum conservation along the $x$ direction leads to the same phase gradient, which yields the equality $(2n-1)\kappa_x = 2\pi/\lambda \sin\theta$. After $\kappa_x$ is substituted by $\gamma$ and $\Lambda$, we arrive at

$$\sin\theta = (2n-1)\frac{\lambda}{\Lambda}\cos\gamma, \tag{2}$$

which indicates that the diffraction angle $\theta$ of transmitted light depends tightly on the operating wavelength and the period of the meta-grating. Considering the extremely small $\gamma$, the item $\cos\gamma$ in equation (2) can be approximated to 1. Equation (2) determines the diffraction behavior (i.e. diffraction angle, orders and efficiency) of the broadband light after passing through the meta-grating. Based on these analysis, we predict that the proposed meta-gratings could create optical vortices with a wavelength-independent phase of $\mathrm{sgn}(x)\beta y$ having its diffraction behavior described by equation (2).

## 3. Experimental verifications

To validate these predictions, we fabricate the meta-grating samples with the parameters $\Lambda = 1$ $\mu$m and $\gamma = \arctan(1/240)$, implying that $\beta = \pi/120$ $\mu\mathrm{m}^{-1}$ and $\kappa_x = 2\pi$ $\mu\mathrm{m}^{-1}$. It indicates that light passing through the meta-grating will have a phase cycle from 0 to $2\pi$ over the distance of 240 $\mu$m in the $y$ direction, which offers an ultrahigh phase accuracy of $\pi/120$ radian per micrometer. Thus, the interval between two neighboring phase singularities is $\tau = 120$ $\mu$m. To facilitate the experimental implementation, we use the apertures with different sizes to create the rational-order optical vortices. To distinguish these optical vortices, we define a parameter $q = d/\tau$, where the diameter $d$ of the aperture changes from 120 $\mu$m to 480 $\mu$m. The parameter $q$ can be used to evaluate the number of phase singularities that are embraced in an aperture. The meta-grating made in a chromium film on a quartz substrate is fabricated by using a standard electron-beam lithography to transfer the meta-grating pattern into the photoresist after the development. Then, a dry etching process is employed to remove the undesired chromium, thus forming the expected devices. Figure 1(b) shows the scanning electron microscope (SEM) image of the fabricated sample, in which we can see high quality gratings are fabricated.

The experimental characterization of its broadband performance is carried out in a confocal configuration of a WITec microscopy system. The experimental intensity profiles captured by a charge-coupled-device (CCD) camera are shown in figure 2(a), where three wavelengths of 488 nm, 532 nm and 633 nm are exemplified as a comparison with the simulated results. Good agreements are observed with highly consistent intensity shape of these optical vortices. However, one can also see that the bilateral symmetry of the two lobes for optical vortices with $q > 1$ is not kept well at different wavelengths. This issue is caused by the fact that the experimental intensity profiles are captured at the Fresnel region, which is different from the Fraunhofer region used in the simulation. During the propagation of a light beam, a Gouy phase arises in terms of $\arctan(z/z_\mathrm{R})$ [17], where $z$ is the distance of propagation, $z_\mathrm{R}$ is the Rayleigh distance. A light beam will undergo a phase delay of $\pi/2$ from $z = 0$ (initial plane) to $z = \infty$ (Fraunhofer distance).

Such a phenomenon also happens in the intensity profiles and phase singularities of an optical beam [18, 19]. To illustrate it in details, we simulate the propagation properties of an optical vortices with $q = 2$ from the initial plane to the Fraunhofer plane. Considering that the beam size will increase as the optical vortices propagate in free space, we cannot simulate the diffraction patterns when the propagating distance $z$ is large. To solve this problem, we utilize a Fourier lens to project the entire Fresnel and Fraunhofer diffraction zone into the region located between the lens plane and the focal plane. The Fourier lens has a phase profile of $\exp(-0.5ikr^2/f)$ [20], where the wavenumber $k = 2\pi/\lambda$, $r$ is the radial coordinate, $f$ is the focal length of the lens. The projection relationship can be mathematically described as $z = fz_0/(f - \mathrm{z}_0)$ [21], where $z$ is the propagation distance of light for the case without the focusing lens, $z_0$ is the propagation distance of light between the lens plane and the correlated plane for the case with the focusing lens. Thus, we obtain the free-space diffraction pattern of a light field at the plane $z$ by using the electric field located at the plane with a distance of $z_0$ from the lens plane. Using the parameters $f = 10$ mm, $\lambda = 532$ nm and the pixel pitch of $400 \times 400$ nm, we simulate the phase and intensity profiles by using the Rayleigh–Sommerfeld diffraction based on a fast-Fourier transform [22]. In figure 2(b), we observe that two phase singularities are located at the $x$ axis at the initial plane ($z = 0$) and then begin to rotate with the propagation of light. At the Fraunhofer region (i.e. the focal plane of the lens), both phase singularities undergo a rotation angle of $\pi/2$, thus changing their locations at the $x$ axis. Since the phase and intensity profiles are highly correlated in an optical beam, the far-field intensity patterns with bilateral symmetry also rotate by an angle of $\pi/2$ (see figure 2(c)), compared with the patterns at the initial plane. Therefore, we can infer that the non-symmetry patterns (e.g. the 488 nm case with $q = 4$) in figure 2(a) might be recorded at the Fresnel region and can be improved further by tuning the position of the CCD detector to the Fraunhofer region. Nevertheless, these experimental

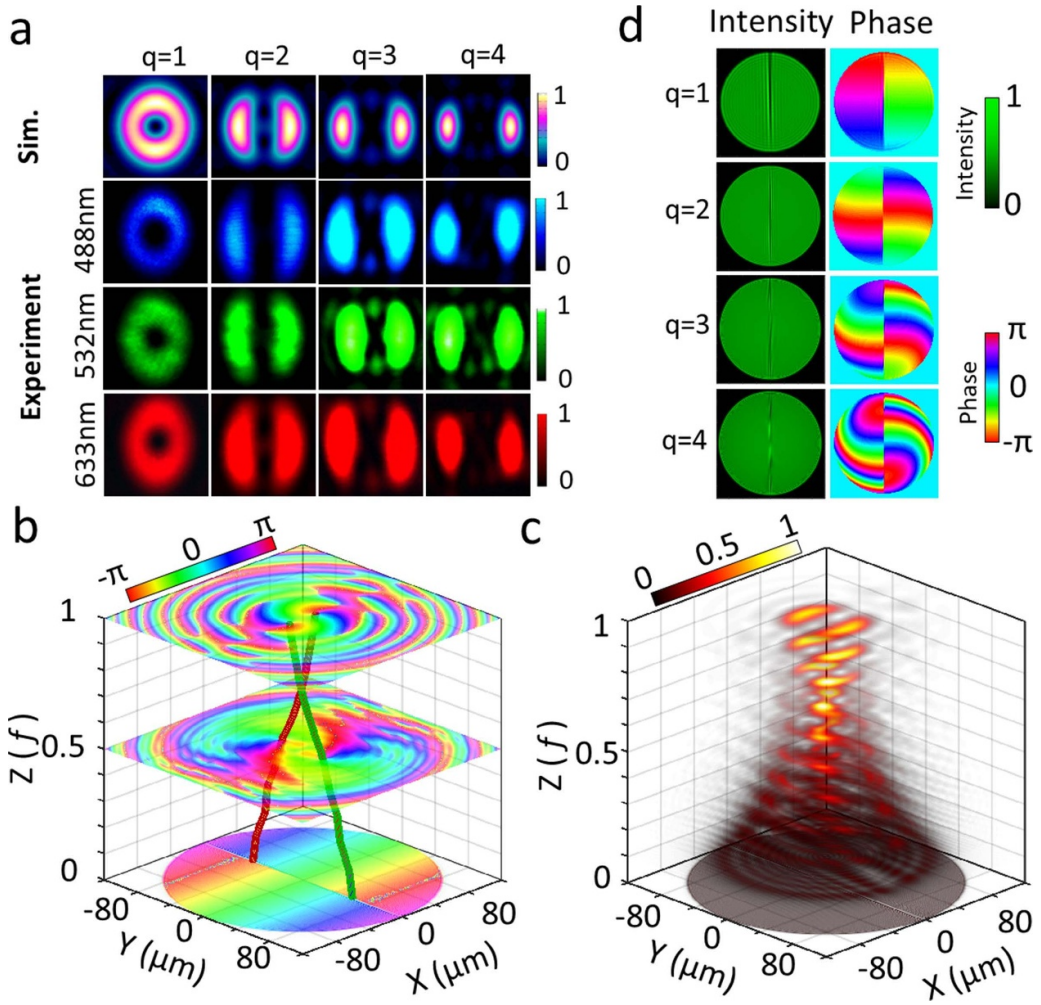


**Figure 2.** (a) Simulated and experimental intensity profiles of optical vortices with $q = 1$–4 at the exemplified wavelengths: 488 nm, 532 nm and 633 nm. (b) Simulated phase profiles at the different $z$-cut planes for an optical vortices with $q = 2$ (the diameter of the aperture is 240 $\mu$m). The phase singularities along its propagation have been labelled in dark red and green for a better discrimination. In the simulation, the meta-grating and the focusing lens with the focal length $f = 1$ cm are located at $z = 0$. (c) Simulated intensity profiles at the $z$-cut planes. The parameters in the simulation are the same with those in (b). (d) The intensity and phase profiles at the imaging plane of a lens with 1 mm long focal length and 700 $\mu$m in diameter. Both the object and image distances are 2 mm, which yields its magnification of 1 to avoid any aberration due to the magnified or shrunk image.

intensity profiles provide sufficient proofs for the broadband creation of optical vortices with different $q$.

In addition, we can also investigate the phase and intensity profiles of these optical vortices at the imaging plane. When imaged by a lens or an objective, the intensity could be reconstructed perfectly for an aberration-free imaging system, but the phase takes an additional parabolic phase. Such the parabolic phase has no influence on the intensity in both theory and experiment, but it cannot be removed in experiment so that the experimental measurement of the phase profiles at the imaging plane is quite challenging. Hence, we merely provide the simulated phase and intensity profiles of these optical vortices at the imaging plane. Figure 2(d) shows the simulated results by using an imaging lens of $f = 1$ mm focal length and 0.7 mm diameter, which is chosen carefully to provide the sufficient power for resolve the details of the encoded phase. Without introducing any additional aberration, we use the imaging magnification of 1, implying that the object and image distances are 2 mm in our simulations. For a better observation of phase singularities at the imaging plane, we remove that parabolic phase ($\exp[-ikr^2/(2f)]$, where $f$ is the focal length of the lens) induced by the imaging process and show the resulting phase in figure 2(d). From the phase at the imaging plane, we can observe the expected phase jump between the left and right parts for these four cases from $q = 1$ to $q = 4$. Although the phase singularities cannot be distinguished clearly in the phase profiles, the intensity profiles reveal the dark regions where the phase singularities are located. Note that, with the increment of $q$, the phase profiles in figure 2(d) have the spiral-like patterns, which might be caused by the incomplete reduction of that additional parabolic phase.

### 3.1. Phase measurement

Figure 3(a) sketches the Mach–Zehnder interferometer used in our experiment for measuring the interference patterns

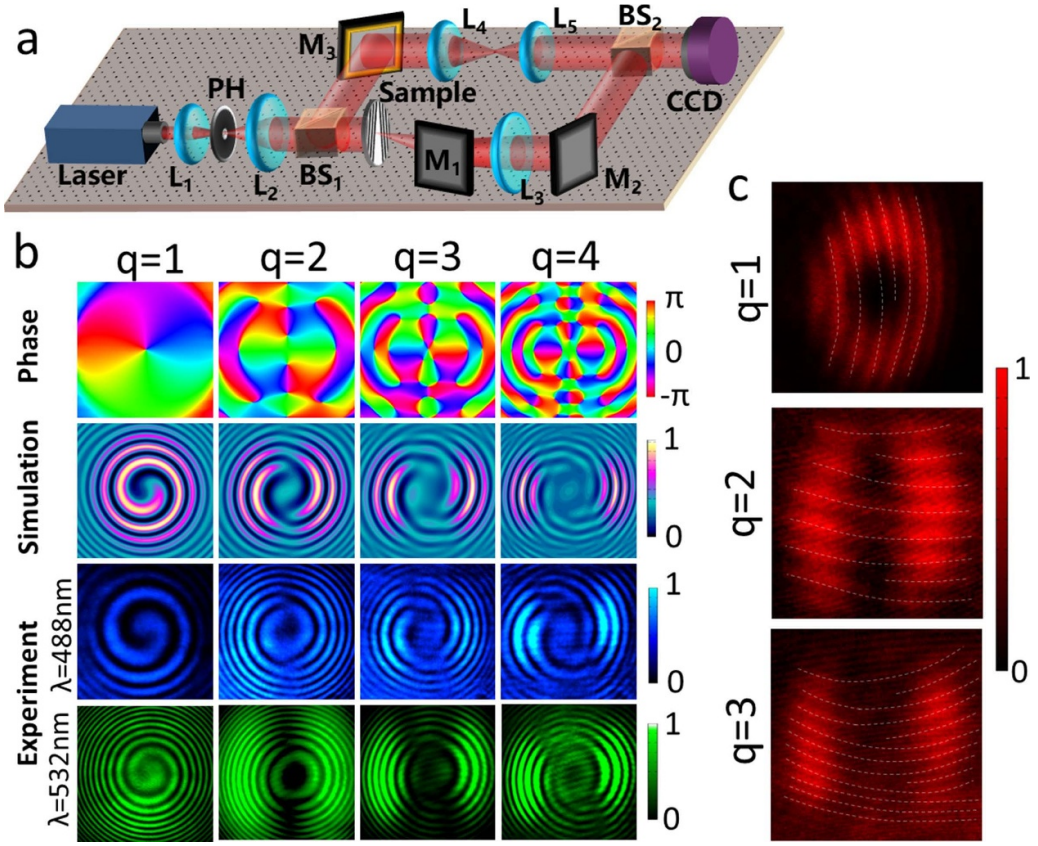


**Figure 3.** (a) Sketch for the experimental setup to measure the interference patterns. PH: pinhole; M: mirror; BS: beam splitter; CCD: charge-coupled device. (b) Simulated phase profiles (first row) of the optical vortices and their interference patterns with the spherical waves (second row). The experimentally recorded interference patterns at the 488 nm (third row) and 532 (forth row) wavelengths are provided for comparison. (c) The experimental fringes of optical vortices interfered with a plane wave at the wavelength of 633 nm. The dashed curves for the case of $q = 3$ are used to guide the fringes for a better observation.

between optical vortices and the reference beam. A laser beam is expanded by a telescopic system composed of two lenses ($L_1$ and $L_2$) and filtered by a pinhole (PH) to obtain a fundamental Gaussian beam. After passing through a beam splitter ($BS_1$), the optical beam is divided into the signal and reference beams. The signal beam is used to illuminate the meta-grating sample for creating optical vortices, which are collimated by the lens $L_3$ to remove the spherical wavefront that arises with the diffraction propagation of the apertured light. The reference beam after the reflection by the mirror ($M_3$) is tuned with a plane or spherical wavefront by using the lenses $L_4$ and $L_5$. The signal and reference beams are combined by the other beam splitter ($BS_2$) to realize the nearly identical propagation direction, thus facilitating the creation of the interference patterns.

The interference patterns recorded by the CCD camera are shown in figure 3(b), where the spiral patterns with their arms dependent on $q$ are observed with high consistency between theory and experiment at the wavelengths of 488 nm and 532 nm. In addition, by using the reference beam with a plane wavefront at the wavelength of 633 nm, we obtain the fork-like fringes where the dislocated parts denote the positions of phase singularities. Caused by the poor coherence of our 633 nm laser, the intensity contrast of the interference fringes at 633 nm wavelength is worse than those at the 488 nm and 532 nm wavelengths. However, it does show the number of dislocated positions that is equal to $q$, which agrees with the simulated phase singularities in figure 3(b). Therefore, both the spiral- and fork-like interference patterns confirms the important phase features of optical vortices at the multiple wavelengths.

### 3.2. *Diffraction orders*

Using equation (2), the maximum diffraction orders are determined by

$$n_{\max} = \mathrm{floor}\left[0.5\Lambda\sin\theta/\left(\lambda\cos\gamma\right) + 0.5\right], \tag{3}$$

where the function floor[$x$] means the integer part of $x$ and $\cos\gamma \approx 1$ due to the small $\gamma$. Figure 4(a) shows the maximum diffraction orders of our meta-gratings with different period under the wavelengths of interest. Since $\sin\theta \leqslant 1$, the transmitted light for the case of $\lambda > \Lambda$ only has the zero-order diffraction, which takes no expected phase as described in equation (1). It denotes that our meta-gratings are only valid at the wavelength smaller than the period of the meta-grating. For our meta-grating of $\Lambda = 1$ $\mu$m in this work, it covers the entire visible wavelengths from 400 nm and 800 nm, where $n_{\max} = 1$ (labelled in dark-yellow color). Thus, in the transmitted light,

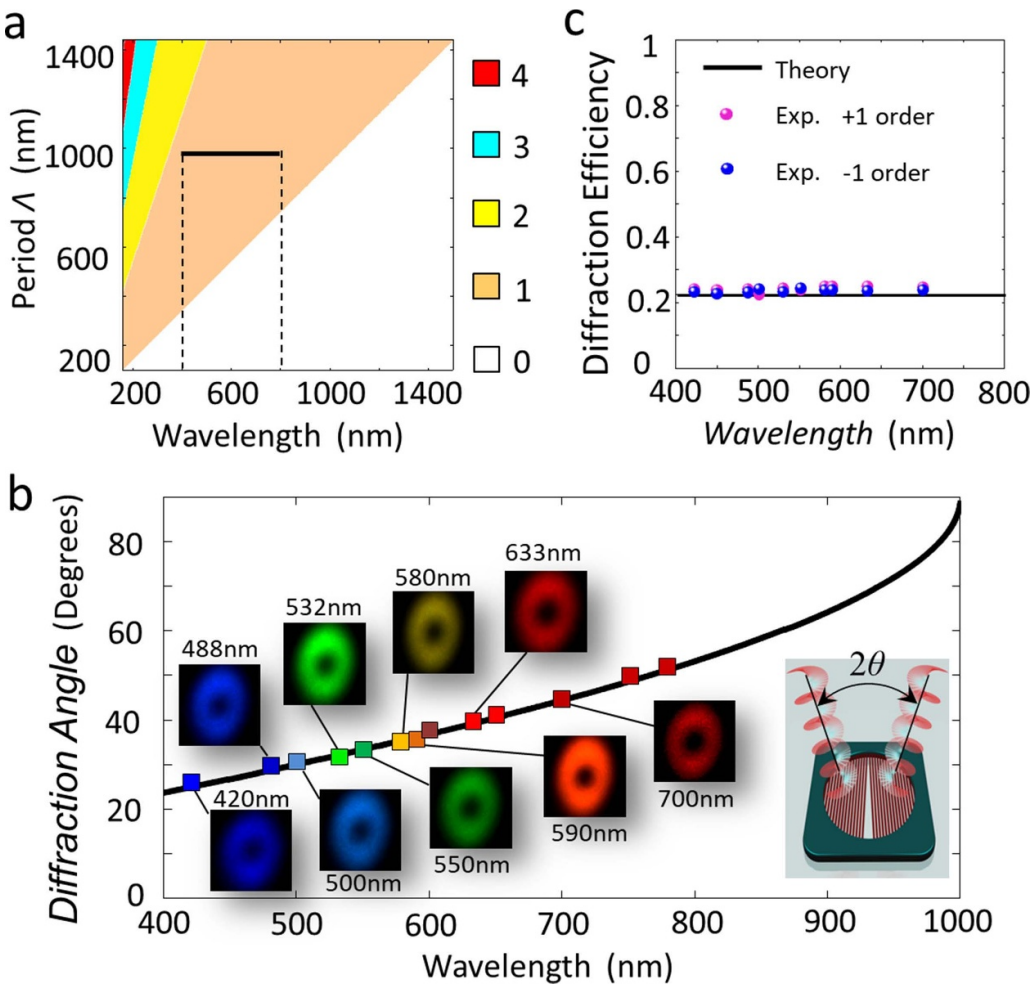


**Figure 4.** (a) Dependence of the largest diffraction orders $n_{max}$ on incident wavelength (λ) and grating period (Λ). The different orders are labelled in colors. In this work, the wavelengths of interest are denoted by the black line, which shows the maximum diffraction order of 1. (b) Measured (squares) and theoretical (line) ±1-order diffraction efficiency of this meta-grating in visible range. (c) Measured (dots) and theoretical (curve) diffraction angle of optical vortices. Insets: (left) experimental intensity profiles for $q = 1$ at different wavelengths; (right) the sketch of the diffraction angle $\theta$.

the meta-gratings yield three diffraction orders: 0 and ±1. As observed in figure 4(a), high diffraction orders will arise for the ultra-violet wavelengths. In addition, because the ratio of the period of meta-grating to the width of the etched slits is 2, our meta-grating could only create the odd-order diffraction, as predicted by the item of $(2n - 1)$ in equation (1). In our meta-grating, the even-order diffraction disappears due to the destructive interference of light transmitted through the etched parts.

Note that one can increase the period Λ of the meta-grating to obtain a large operating bandwidth, as sketched in figure 4(a). However, the large Λ leads to the small diffraction angle (see equation (3) and the following section) so that more high-order diffraction appear and the efficiency of every order decreases. In principle, the period Λ has the maximum value so that the 0-order and 1-order beams are not overlain with each other during the propagation. Due to the diffraction effect, both the 0-order and 1-order beams expand the lateral size in a divergent angle of $\Delta\theta = 1.22\lambda/R$, where $R$ is the radius of a circular-shaped beam and is equal to the radius of the aperture here. Thus, we can derive that the minimum diffraction angle of the 1-order beam equals $1.22\lambda/R = \theta_{min} \approx \lambda/\Lambda_{max}\cos\gamma$, yielding the maximum period $\Lambda_{max} \approx R{\cdot}\cos\gamma/1.22$. This means that the period of the meta-grating should not larger than $0.8R$, which guarantees that at least 2.5 periods are located within the circular aperture (with a radius of $R$) of the meta-grating. In fact, such a period $\Lambda_{max}$ can be satisfied easily in real applications. Thus, we have the period of the meta-grating with the range of $\lambda < \Lambda < R{\cdot}\cos\gamma/1.22$.

### 3.3. Diffraction angle

Although the reported meta-grating operates in broadband, the diffraction angles are different with high dependence on the wavelength. To reveal it, we rewrite equation (2) as $\sin\theta = \lambda/\Lambda$, where $n = 1$ and $\cos\gamma \approx 1$ are used for ±1-order diffraction. At the operating spectrum, light with longer wavelength has a large diffraction angle, as sketched theoretically in figure 4(b). Note that such a wavelength-dependent relationship holds for all the optical vortices with different $q$. Hence,

the diffraction angles of optical vortices with $q = 1$ are demonstrated experimentally as an example to verify the relationship. Figure 4(b) shows the measured diffraction angles and the intensity profiles of optical vortices with $q = 1$ at the exemplified wavelengths from 420 nm to 780 nm. A supercontinuum light source (SuperK Fianium) is used in the experiment to generate different wavelengths that are filtered by an acousto-optic modulator (NKT, Photonics). The nearly perfect consistence between experiment and theoretical prediction has been achieved. In the insert of figure 4(b), the measured intensity profiles with the doughnut shape for $q = 1$ are nearly identical at the different wavelengths, which indicates that our proposed device yields the identical phase, as expected.

Since the period $\Lambda = 1$ is used in our work, the diffraction angle is fixed at the given wavelength. In fact, the angle of the first-order diffraction increases with the decrement of the period. Considering that the operating wavelength must be smaller than the period $\Lambda$ of the meta-grating, our vortices have the maximum diffraction angle of 90°. Therefore, the diffraction angle has the tight dependence on the wavelength and the period of the meta-grating.

### 3.4. Diffraction efficiency

According to the above analysis, our meta-grating has only 0-order and ±1-order diffraction. We consider their diffraction efficiency $\eta_j = I_j/(\sum I_j)$, where $j = 0, \pm 1$ and $I_j$ is the intensity of $j$th order diffraction. Theoretically, from equation (1), the intensity $I_j$ ($j = 0, \pm 1$) can be obtained by $I_j = |A_j|^2$, where $A_0 = 0.5$, $A_{\pm 1} = 0.5\mathrm{sinc}(1/2) = 0.3183$, leading to $\eta_{\pm 1} = 22.38\%$, which is wavelength-independent. Note that, the above results are obtained under the assumption that $I_j$ contains all the power of its own diffraction order. Figure 4(c) shows the measured diffraction efficiency with the nearly constant values at the different wavelengths. The slight derivation between experiment and simulation might be caused by the inaccuracy of the measured intensity profiles due to the scattering of light and the limited size (∼1 cm in diameter) of the detector.

The maximum diffraction efficiency of our device is obtained when only three orders (i.e. 0 and ±1 orders) exist in the transmitted light. Considering that the coefficient $A_j$ is fixed for all the orders, the diffraction efficiency of the first order will decrease if more orders are created, because the denominator in the definition increases. In addition, the higher-order diffraction has the $jq$-index phase profile, where $j$ denotes the diffraction order and $q = d/\tau$ for $j = 1$. It means that the distance between two neighboring phase singularities at the $j$-order diffraction is shorten to be $\tau/j$. However, the efficiency of higher-order diffraction is quite low because the $A_j$ decreases for a large $j$. Therefore, only the first-order diffraction is useful in practical applications.

## 4. Discussions

Due to the binary-amplitude feature of our meta-grating, it has the maximum total efficiency of ∼10% [20], which is defined as the ratio of the power of optical vortex beam to the total power of the incident beam. To enhance it, our meta-gratings can be made with multi-level phase on a transparent substrate, which theoretically allows for the maximum total efficiency approaching 100% when the phase level is high enough. Note that, the efficiency of the phase-type meta-gratings is the highest only at the designed wavelength but it reduces when the illuminating wavelength is deviated. Nevertheless, the phase-type meta-gratings still have higher efficiency than the amplitude-type meta-gratings. To create the spiniform phase that is critical in realizing these rational-order optical vortices, one can also use other phase encoding techniques such as optical geometric metasurfaces [23] and phase-type spatial light modulators (SLMs) [24], instead of the meta-gratings. However, both metasurfaces and SLMs have limited bandwidth to create optical vortices. From fabrication point of view, our meta-grating is less challenging and can be fabricated at the wafer level by existing semiconductor technology. Therefore, a balance between the device performance, fabrication, reconfigurability and integration should be carefully made before creating such rational-order optical vortices in practical applications.

The vortices from our bilateral meta-grating have the average OAM per a photon by a relationship [15]:

$$Q = 0.7q - \sin(\pi q/2)\,\mathrm{sinc}(\pi q/2)/2, \tag{4}$$

where $Q$ is the calculated OAM, both $q$ and $Q$ can take any rational value. They can be taken as a weighted superposition of the orthogonal vortex modes, so both the phase and intensity profiles undergo a significant variation during their propagation in free space, which behaves like the fractional-order Lauguerre–Gaussian beams. Although we only report the broadband properties of optical vortices with the integer $q$, the non-integer-$q$ vortices shall have similar properties as they are generated simply by changing the diameter of the sample aperture, which has no influence on the structure of meta-grating, optical efficiency, diffraction angle and orders. Since the reported vortices control the topological charges via the number of the phase singularities, their topological charges always take the integer values while the whole optical beam has the rational OAM of $Q$ [15]. This property is distinguished from the traditional Laguerre–Gaussian or Bessel–Gaussian beams with the phase of $e^{im\varphi}$, where the topological charge $m$ can take the fractional value (i.e. $m_f$).

## 5. Conclusion

In summary, we have reported the broadband creation of rational-order optical vortices by using a bilateral meta-grating. Based on the mathematical analysis, we theoretically predict the broadband behaviors of the meta-gratings. The experimental intensity profiles and interference fringes of optical vortices with integer $q$ at the exemplified wavelengths show good agreement with the numerical simulations. The diffraction angle, orders and efficiency of the meta-gratings

are confirmed experimentally at the visible spectrum, exhibiting the broadband feature. The meta-grating based rational-order optical vortex generator is promising for applications in optical micro-manipulation, communication and quantum physics, and can be extended to the creation of vortices for other electromagnetic waves, acoustic waves [25] and matter waves [26].

## Acknowledgments

K H thanks CAS Pioneer Hundred Talents Program, 'the Fundamental Research Funds for the Central Universities' in China, the National Natural Science Foundation of China (Grant Nos. 61875181 and 61705085), USTC Research Funds of the Double First-Class Initiative (Grant No. YD2030002003), and the support from the University of Science and Technology of China's Centre for Micro and Nanoscale Research and Fabrication. J T thanks the support from the Agency for Science, Technology and Research (A*STAR) under AME IRG Grant No. A2083c0058.

## ORCID iD

Kun Huang https://orcid.org/0000-0002-9391-149X

## References

[1] Andrews D L and Babiker M 2012 *The Angular Momentum of Light* (Cambridge: Cambridge University Press)
[2] Beth R A 1936 *Phys. Rev.* **50** 115
[3] Ling X, Zhou X, Huang K, Liu Y, Qiu C-W, Luo H and Wen S 2017 *Rep. Prog. Phys.* **80** 066401
[4] Bliokh K Y, Rodriguez-Fortuno F J, Nori F and Zayats A V 2015 *Nat. Photon.* **9** 796–808
[5] Huang K *et al* 2016 *Laser Photonics Rev.* **10** 500–9
[6] Berova N, Nakanishi K and Woody R W 2000 *Circular Dichroism: Principles and Applications* (New York: Wiley)
[7] Allen L, Beijersbergen M, Spreeuw R and Woerdman J 1992 *Phys. Rev.* A **45** 8185–9
[8] Wang J, Yang J-Y, Fazal I M, Ahmed N, Yan Y, Huang H, Ren Y, Yue Y, Dolinar S and Tur M 2012 *Nat. Photon.* **6** 488–96
[9] Gong L, Zhao Q, Zhang H, Hu X-Y, Huang K, Yang J-M and Li Y-M 2019 *Light: Sci. Appl.* **8** 27
[10] Mair A, Vaziri A, Weihs G and Zeilinger A 2001 *Nature* **412** 313–6
[11] Dada A C, Leach J, Buller G S, Padgett M J and Andersson E 2011 *Nat. Phys.* **7** 677–80
[12] Curtis J E and Grier D G 2003 *Phys. Rev. Lett.* **90** 133901
[13] Chen L, Lei J and Romero J 2014 *Light: Sci. Appl.* **3** e153
[14] Berry M 2004 *J. Opt. A: Pure Appl. Opt.* **6** 259
[15] Huang K, Liu H, Restuccia S, Mehmood M Q, Mei S, Giovannini D, Danner A, Padgett M J, Teng J and Qiu C-W 2018 *Light: Sci. Appl.* **7** 17156
[16] Garcia-Vidal F J, Martin-Moreno L, Ebbesen T W and Kuipers L 2010 *Rev. Mod. Phys.* **82** 729–87
[17] Kogelnik H and Li T 1966 *Appl. Opt.* **5** 1550–67
[18] Davis J A and Bentley J B 2005 *Opt. Lett.* **30** 3204–6
[19] Wang X-L, Lou K, Chen J, Gu B, Li Y and Wang H-T 2011 *Phys. Rev.* A **83** 063813
[20] Goodman J W 2005 *Introduction to Fourier Optics* (Greenwoood Village: Roberts and Company Publishers)
[21] Huang K, Gao H F, Cao G W, Shi P, Zhang X B and Li Y 2012 *Appl. Opt.* **51** 5149–53
[22] Huang K, Qin F, Liu H, Ye H, Qiu C W, Hong M, Luk'yanchuk B and Teng J 2018 *Adv. Mater.* **30** 1704556
[23] Zhang L, Mei S, Huang K and Qiu C-W 2016 *Adv. Opt. Mater.* **4** 818–33
[24] Maurer C, Jesacher A, Bernet S and Ritsch-Marte M 2010 *Laser Photonics Rev.* **5** 81–101
[25] Melde K, Mark A G, Qiu T and Fischer P 2016 *Nature* **537** 518–22
[26] McMorran B J, Agrawal A, Anderson I M, Herzing A A, Lezec H J, McClelland J J and Unguris J 2011 *Science* **331** 192–5